TISSUE ENGINEERING: Part A
Volume 17, Numbers 7 and 8, 2011

DOI: 10.1089/ten.tea.2010.0275

Effects of Extracellular Matrix Density and Mesenchymal Stem Cells on Neovascularization *In Vivo*

Ekaterina Kniazeva, M.S.,[1] Suraj Kachgal, M.S.,[1,2] and Andrew J. Putnam, Ph.D.[2]

Aberrant angiogenesis is common to a variety of diseases in which alterations in tissue mechanical properties also occur. A fundamental understanding of the interdependence of angiogenesis and tissue structural properties may enhance the development of therapeutic strategies. We previously established that increasing extracellular matrix density inhibits capillary morphogenesis in three-dimensional tissues *in vitro*, and that addition of human mesenchymal stem cells (MSCs) partially rescues a healthy angiogenic phenotype. This study's goal was to investigate if these effects can be recapitulated *in vivo.* Human umbilical vein endothelial cells, MSCs, or a mixture of both was suspended in fibrin gel precursor solutions of 5, 10, and 15 mg/mL concentrations and injected subcutaneously into SCID mice. Neovascularization was assessed in tissue constructs retrieved at 3, 7, and 21 days by quantifying vessel numbers, perfusion, thickness, maturity, and perivascular collagen deposition. The data show that changing extracellular matrix density inhibits capillary morphogenesis *in vivo* in a manner consistent with that observed *in vitro.* Delivery of both human umbilical vein endothelial cells and MSCs produced more robust and mature vessels than delivery of either cell type alone in all tissue concentrations.

Introduction

A number of pathologies are characterized by inadequate blood vessel growth and, consequently, insufficient nutrient supply to adjacent tissues. Therapeutic angiogenesis via gene, protein, or cell delivery attempts to combat this insufficiency by promoting neovascularization.[1–4] Understanding the fundamental role of the extracellular matrix (ECM) as a physical barrier to neovascularization may enhance efforts to develop new approaches that promote healthy and abundant vessel formation. A number of studies have demonstrated that ECM density and mechanical properties play significant roles in regulating capillary morphogenesis *in vitro.* On two-dimensional (2D) culture substrates, *in vitro* studies provide evidence that ECM ligand density can control growth and morphology of capillary formation[5] and that mechanical cues impact tubulogenesis.[6–8]

In three-dimensional (3D) tissues, our lab and others have shown that angiogenic processes *in vitro* may also depend on mechanical properties of the surrounding interstitial matrix. To investigate the contributions of tissue dimensionality and mechanical properties, we previously adopted a fibrin-based model of angiogenesis, first described by Nehls and Drenckhahn.[9] In this model system, human umbilical vein endothelial cells (HUVECs) form capillary-like structures in 3D when cocultured with a supporting mesenchymal cell type, such as normal human lung fibroblasts[10] or bone-marrow-derived mesenchymal stem cells (MSCs),[11] both of which secrete proangiogenic factors. In our prior studies, we demonstrated that when the mesenchymal support cells were cultured on top of the fibrin gel, a fixed distance away from the HUVEC-coated microcarrier beads, increasing ECM density significantly inhibited angiogenic sprouting and the formation of capillary vessels *in* vitro.[10–12] Mechanistically, the inhibition caused by elevated ECM density is partially related to the HUVECs' inability to upregulate key matrix metalloproteinases (MMPs), including MMP-2, MMP-9, and MT1-MMP, which are necessary for successful remodeling of the fibrin matrix. In addition, increased ECM density significantly impeded diffusive transport.[10] However, when either normal human lung fibroblasts or MSCs were distributed within the hydrogel, they delivered proangiogenic factors closer to the HUVECs, adopted a pericyte-like phenotype, and improved the angiogenic phenotype of the HUVECs even in denser matrices.[11,13]

On the basis of our prior *in vitro* results, the primary objective of this study was to investigate the influence of ECM density on capillary formation *in vivo,* and to assess the ability of MSCs to stimulate functional vessels within dense 3D fibrin matrices *in vivo.* To accomplish this goal, fibrin gel precursor solutions of varied protein concentrations of 5, 10, or 15 mg/mL containing mixtures of HUVECs and/or MSCs

[1]Department of Biomedical Engineering, University of California, Irvine, Irvine, California.
[2]Department of Biomedical Engineering, University of Michigan, Ann Arbor, Michigan.

were injected subcutaneously in SCID mice. Tissue constructs were retrieved at various time points, and the engineered blood vessels present within tissue sections were then evaluated in terms of quantity, perfusion, thickness, stimulation of collagen production, and MSC differentiation toward a smooth muscle cell phenotype. A definitive relationship between tissue density and capillary morphogenesis *in vivo* was identified, and the ability of MSCs to support formation of more functional and mature capillary networks, regardless of tissue density, was demonstrated.

Materials and Methods

Cell culture

Human MSCs from human bone marrow (Lonza, Walkersville, MD) were cultured in Dulbecco's modified Eagle's medium (Sigma-Aldrich, St. Louis, MO) supplemented with 10% fetal bovine serum (Mediatech, Manassas, VA), 1% penicillin/streptomycin (Mediatech), and 0.5% gentamicin (Invitrogen, Carlsbad, CA) at 37°C, 5% CO_2 and used up to passage 13. HUVECs were isolated from fresh umbilical cords as described previously,[14] cultured in fully supplemented endothelial growth medium (EGM-2; Lonza), and used at passage 2. The medium was changed three times per week, and cells were harvested at 80% confluency via trypsin-EDTA (Mediatech) treatment.

Tissue construct implantation and retrieval

Animal procedures were performed in accordance with NIH guidelines for laboratory animal usage following a protocol approved by UC Irvine's Institutional Animal Care and Use Committee (IACUC). C.B-17/SCID male mice (Taconic, Hudson, NY) aged 8 weeks were used for all experiments. A prepared anesthetic/analgesic cocktail of ketamine (95 mg/kg), xylazine (9.5 mg/kg), and buprenorphine (0.059 mg/kg) (Western Medical Supply, Arcadia, CA) was delivered via an intraperitoneal injection. The dorsal area of each animal was subsequently shaved and sterilized with betadine (Thermo Fisher Scientific, Fremont, CA) before injection of the implant solution.

Fibrinogen (Sigma-Aldrich) solutions of 5, 10, and 15 mg/mL concentrations were prepared in serum-free EGM-2 and sterile filtered. Mixtures of cells necessary for implant constructs were spun down for 5 min at 200 *g* and re-suspended in appropriate fibrinogen solutions at concentration of 1 million cells per 100 μL of solution. Just before injection, 5% fetal bovine serum and 6 μL of a thrombin (Sigma-Aldrich) solution (50 U/mL) were added to 300 μL of the fibrinogen solution and immediately injected subcutaneously on the dorsal surface of the SCID mouse, two implants per animal. While the implant polymerized, the animal was kept stationary for 5 min and subsequently placed in the recovery cage. Testing conditions for fibrin implants included triplicates of acellular, MSC only, HUVEC only, and MSC/HUVEC cell mixture conditions in varied fibrin concentrations of 5, 10, and 15 mg/mL, which were retrieved at 3, 7, and 21 days, amounting to a total of 54 mice or 108 samples (Table 1). At each retrieval time point, the animals were euthanized and implants including surrounding skin and muscle layers surgically removed.

Immunohistochemical explant processing

Explants were first fixed in 10% formalin solution overnight, transferred to PBS solution, and then forwarded to AML Laboratories (Rosedale, MD) for paraffin embedding and sectioning. Five-micrometer sections were then deparaffinized, rehydrated, and incubated in Target Retrieval solution (Dako, Carpinteria, CA) for 25 min at 98°C. Immunohistochemical staining was performed with Dako EnVision System-HRP (DAB) kit. Overnight incubation using anti-human CD31 primary antibody diluted at 1:50 (Dako) or anti-human calponin at 1:50 dilution (Santa Cruz Biotechnology, Santa Cruz, CA) was followed by treatment with HRP-conjugated anti-mouse secondary antibody provided in the kit, and hematoxylin and eosin counterstain. Negative controls involving staining with the secondary antibody alone were generated for all samples to rule out the possibility of nonspecific staining. All sections were also stained using a trichrome kit (ScyTek Laboratories, Logan, UT) according to the provided protocol.

Imaging and statistics

Stained tissue sections were imaged using a Nikon Eclipse E800 microscope system at 400× magnification. All digital images obtained were numerically coded and all identifiable markers removed to blind the researchers during the counting and measuring procedures. For each histomorphometry metric, 10 randomly selected fields of view were analyzed within the fibrin implant on each section. Data from these 10 randomly selected fields of view were compiled for each of three independent explanted samples for each condition tested. The resulting data reported represent mean ± standard deviation ($n = 3$, with 10 images per sample), and were statistically analyzed and represented using KaleidaGraph (Synergy Software). A one-way analysis of variance was performed to obtain statistical significance comparisons among data sets. Statistical significance was assumed when $p < 0.05$. To facilitate understanding and interpretation of the data, and to more easily observe different statistical comparisons, the resulting figures portray the same data sets in two different ways: as a function of both fibrin concentration and cell condition.

Table 1. Summary of Experimental Conditions

Cell type	*Acellular*	*HUVECs*	*MSCs*	*HUVECs+ MSCs*
5 mg/mL fibrin	—	3 million/300 μL gel	3 million/300 μL gel	1.5+1.5 million/300 μL gel
10 mg/mL fibrin	—	3 million/300 μL gel	3 million/300 μL gel	1.5+1.5 million/300 μL gel
15 mg/mL fibrin	—	3 million/300 μL gel	3 million/300 μL gel	1.5+1.5 million/300 μL gel

HUVECs, human umbilical vein endothelial cells; MSCs, mesenchymal stem cells.

Results

Lumen formation and quantification of baseline vascularization levels

To establish a baseline level for the total number of blood vessel-like structures formed within the implants, implanted tissues retrieved at specific time points were first evaluated by quantifying the number of structures with clearly identifiable lumens in each condition. The overall gross morphology of a typical fibrin implant in the subcutaneous space is shown in Figure 1A; examples of lumen-containing structures that were counted to generate quantitative data are shown as well. A second exemplary explant (Fig. 1B) shows the typical organization seen in these experiments, including skin, muscle, and fatty layers of the mouse tissue surrounding the fibrin implant (marked F on the image). While the thickness of the explants decreased slightly over time, this organization remained uniform for all conditions. Neovessels were characterized by the presence of hollow lumen structures (Fig. 1C), which were evaluated for all conditions in these experiments. Baseline quantification of all lumen-containing structures, excluding structures that appeared to be cells coalescing together but which have not yet formed a hollow lumen in these studies, is shown in Figure 2A–F. Significantly higher levels of capillary structures were observed in 5 mg/mL fibrin gel implants containing both HUVECs and MSCs; however, in tissues fabricated from 10 and 15 mg/mL fibrin, implants containing HUVECs only exhibited higher numbers of lumens than did those containing both HUVECs and MSCs combined. In addition, the total number of lumen-containing structures was higher in lower ECM densities for all cell conditions. The overall size of the implants decreased over time due to the degradation of the fibrin hydrogels, a process previously shown to be required for capillary morphogenesis.[11,13] However, because the data reported here represent total numbers of vessels per field of view, rather than vessel density (i.e., numbers of vessels per implant area), the shrinking size of the implants did not impact the quantitative results.

It was also necessary to identify the total number of vessels with clearly defined lumens that were formed by the implanted human cells, as opposed to those formed by infiltrating mouse cells. To distinguish implanted cells, the sections were stained with anti-human CD31 antibody, which identified HUVECs within the tissues (Fig. 3). The resulting sections were imaged and the total numbers of human CD31-positive structures with clearly identifiable lumens were counted. Quantification of these data supported our previous observation that enhanced vessel formation was achieved in fibrin gels of lower protein concentrations. These data were evaluated only in implants containing HUVECs or HUVECs+MSCs (Fig. 3A–E), as the implants containing only MSCs (i.e., lacking HUVECs) did not exhibit any positive human CD31 staining, as expected (data not shown).

Vessel maturity evaluation via perfusion and vessel diameter quantification

Once the baseline quantities of vessels formed by the implanted cell types were established, any differences in maturity, phenotype, and functionality of these newly formed vessels were characterized. To evaluate functionality of these vessels, the numbers of vessel lumens perfused with red

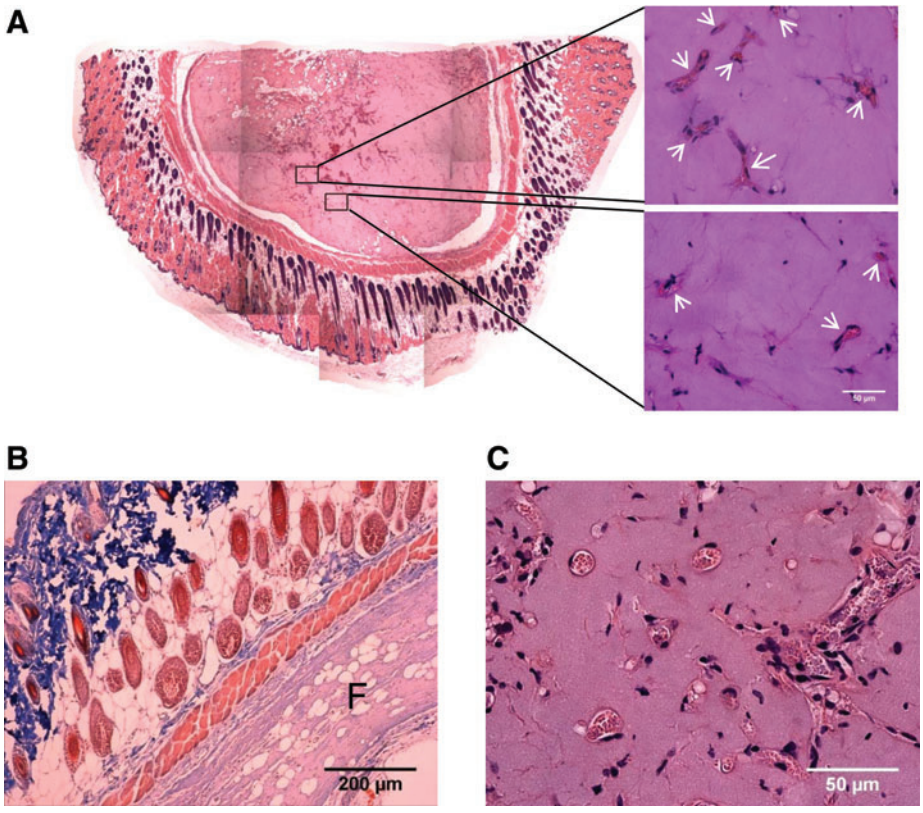

FIG. 1. The methods to characterize fibrin-based implants and neovascularization are depicted. **(A)** A compilation of images stitched together reveals the gross morphology of a typical fibrin implant (left). Candidate vessel structures identified by the presence of well-defined lumens (arrowheads, right) were counted to yield a quantitative metric of vessel formation. Higher magnification images show **(B)** typical implant orientation relative to the subcutaneous mouse tissue (F identifies fibrin) and **(C)** examples of lumen-containing structures that were quantified. Color images available online at www.liebertonline.com/tea.

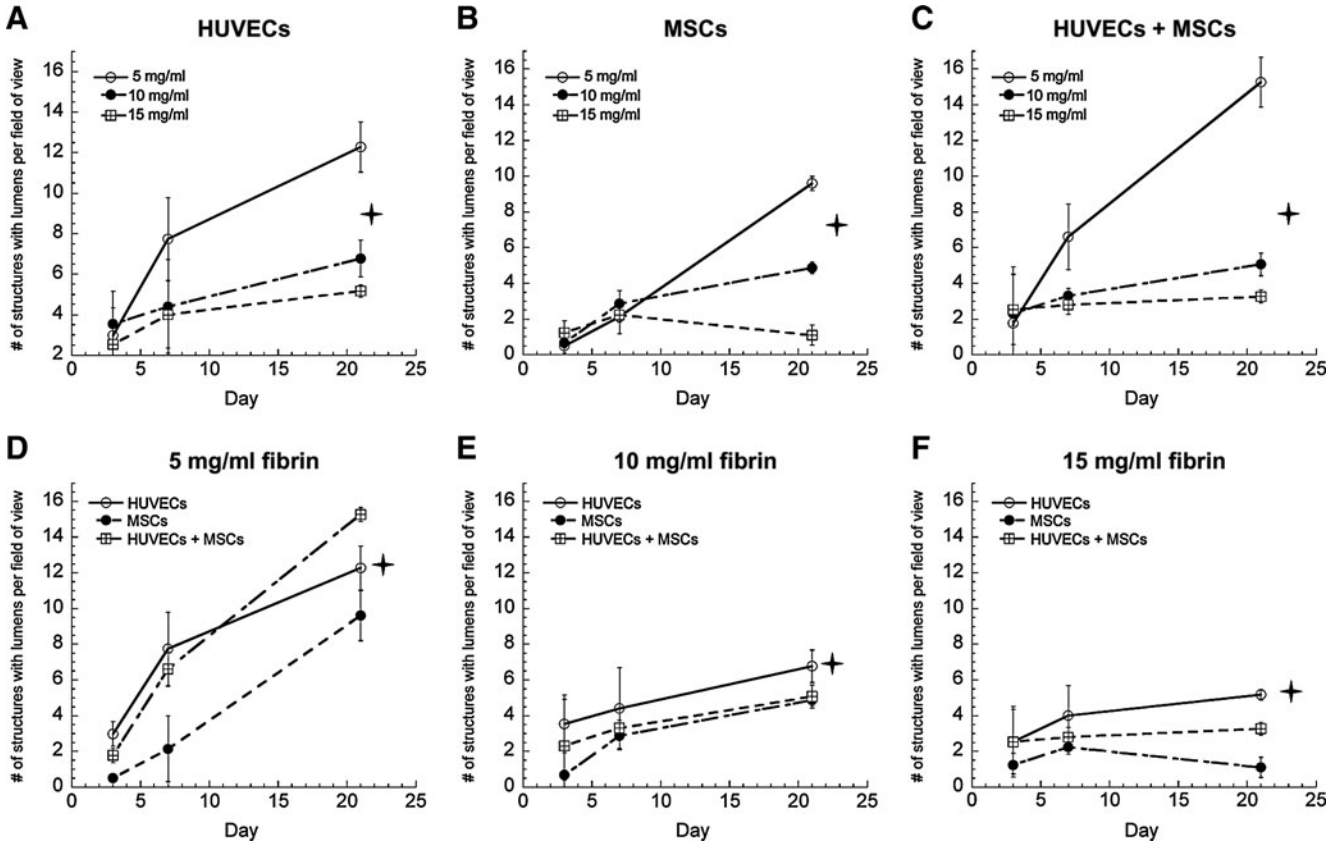

FIG. 2. Quantification of the numbers of lumen-containing structures in tissue constructs containing **(A)** HUVECs only, **(B)** MSCs only, or **(C)** HUVECs+MSCs in 5 (O), 10 (•), and 15 mg/mL (□) fibrin-based implants. The same data are also represented for **(D)** 5 mg/mL fibrin, **(E)** 10 mg/mL fibrin, **(F)** 15 mg/mL fibrin as a function of the cellular conditions, with HUVECs alone (O), MSCs alone (•), or HUVECs+MSCs (□) at days 3, 7, and 21. For panels **(A–C)**, the star symbol (✦) denotes a statistically significant relationship ($p < 0.05$) between each data set at day 21; for panels **(D–F)**, ✦ indicates a statistically significant relationship ($p < 0.05$) between the HUVEC-only condition (O) and the other two cell conditions at day 21. HUVECs, human umbilical vein endothelial cells; MSCs, mesenchymal stem cells.

blood cells were quantified. CD31-stained tissue constructs formed using 5 mg/mL fibrin contained the highest numbers of perfused vessels in all cell conditions, and codelivery of HUVECs and MSCs led to the greatest number of perfused vessels across all ECM densities (Fig. 4A–E). Implants containing HUVECs alone or MSCs alone were similar in terms of the number of perfused structures. However, gels containing HUVECs alone exhibited more leaky vessels, marked by the presence of red blood cells not confined within clearly identifiable hollow lumens but rather dispersed throughout the extracellular space (Fig. 4F, G, asterisks mark extravascular red blood cells). Quantification of lumen diameters also revealed larger vessels in coimplant conditions, ranging from about 18 μm in 5 mg/mL fibrin gels down to 11 μm in 15 mg/mL fibrin gels (Fig. 5A–F). Larger vessels were also predominantly present in all conditions in lower ECM densities (Fig. 5G–I), supporting the argument that higher ECM density impedes vessel maturation.

Collagen deposition and MSC differentiation into stabilizing pericytes

To further assess vessel development and stability, perivascular collagen deposition, which identifies more mature and well-supported vessels capable of producing their own ECM, was assessed in histological sections. A trichrome stain revealed higher collagen deposition around nascent vessel structures in tissues fabricated with lower density fibrin gels, as well as in coculture conditions in all ECM concentrations (Fig. 6A–G). Tissue sections were also stained for human-specific calponin, a marker of smooth muscle differentiation, to determine if the implanted MSCs differentiated toward a stabilizing pericyte phenotype around the nascent vessels. Larger numbers of human calponin-positive structures were observed in the lower density fibrin gels (Fig. 7A–C), and were also more prevalent in implants containing both HUVECs and MSCs (Fig. 7D, E).

Discussion

This study explored the relationship between ECM density and capillary morphogenesis *in vivo*, and examined the potential of MSCs to promote vessel development in fibrin implants of increasing density. In previous studies using a 3D fibrin-based *in vitro* model, we demonstrated that capillary morphogenesis was significantly reduced by increasing ECM density, and that it could be partially restored by distributing MSCs throughout the tissue.[11] This suggested a

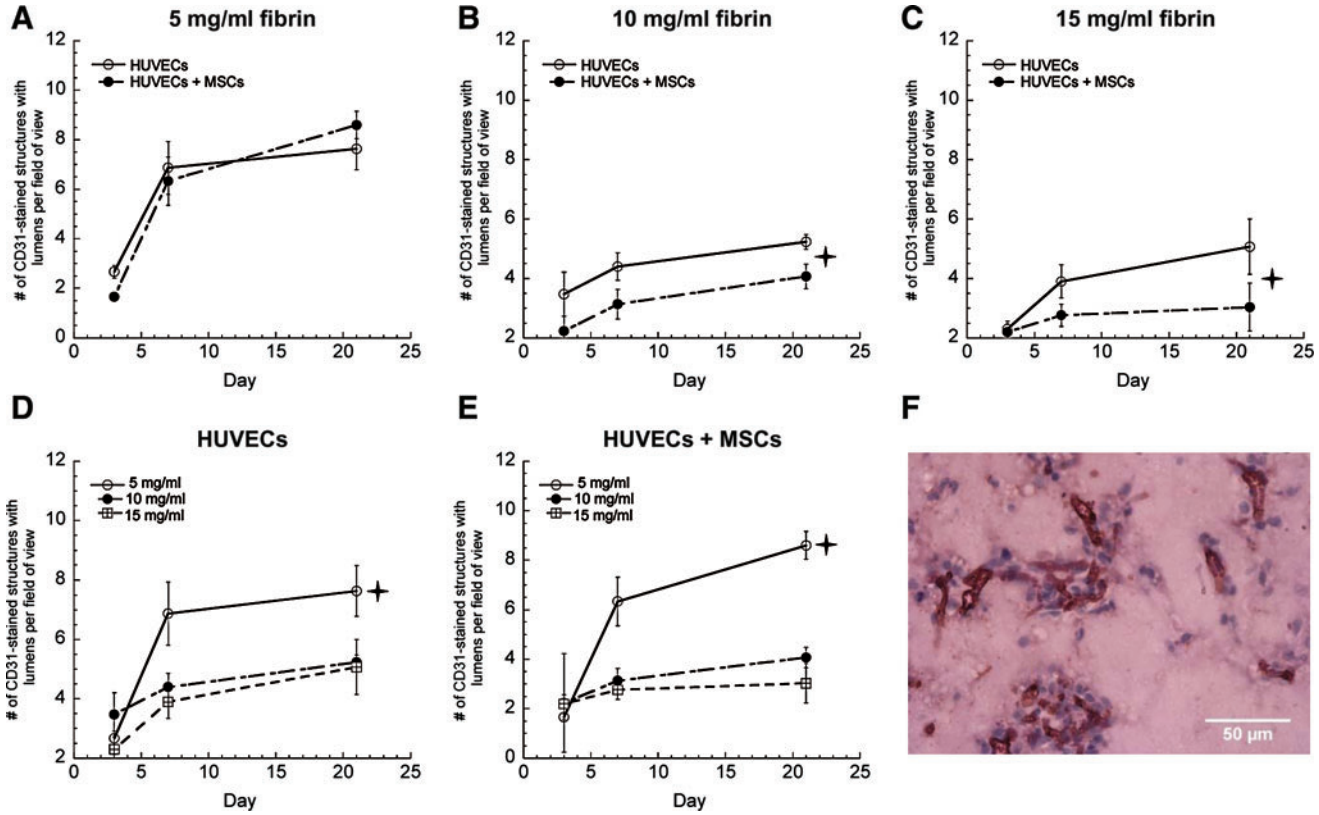

FIG. 3. Vessel structures stained positive for human CD31 in tissue constructs comprised of **(A)** 5 mg/mL fibrin, **(B)** 10 mg/mL fibrin, **(C)** 15 mg/mL fibrin with either HUVECs alone (O) or HUVECs+MSCs (●). For panels **(B** and **C)**, ✦ indicates statistically significant differences between the two data sets at day 21 ($p < 0.05$). Data are also presented as a function of fibrin concentration **(D)** HUVECs only, **(E)** HUVECs+MSCs in 5 (O), 10 (●), and 15 mg/mL (□) fibrin-based implants at days 3, 7, and 21; ✦ indicates a statistically significant difference ($p < 0.05$) between 5 mg/mL and the other two fibrin concentrations at day 21. **(F)** A representative human CD31-stained construct at day 21 in 15 mg/mL fibrin with HUVECs only. Color images available online at www.liebertonline.com/tea.

means to overcome restrictions on the diffusive transport of large macromolecules imposed by elevated matrix density.[10] Changes in fibrin concentration simultaneously influence ECM mechanical properties,[11] adhesive ligand density, and proteolytic sensitivity, all of which could act as instructive cues that regulate capillary morphogenesis. Nevertheless, whether the ECM's effects on capillary morphogenesis are chemical, mechanical, or both, the relevance of these prior *in vitro* observations for vascularization *in vivo* remained unclear, and motivated this study. The important contributions of the current study are the demonstration that elevated fibrin matrix density inhibited the formation of vasculature *in vivo* much as it does *in vitro*, and that this inhibition can be partially remedied by codelivering MSCs with HUVECs.

With respect to the first contribution, the data presented show that matrix density plays a critical role in regulating neovascularization *in vivo.* A significant reduction in the total numbers of lumen-containing structures was observed in 10 and 15 mg/mL fibrin tissues as compared to 5 mg/mL samples for all conditions (Fig. 2). In addition, ECM density was also found to regulate vessel perfusion (Fig. 4), size (Fig. 5), perivascular collagen deposition (Fig. 6), and MSC differentiation (Fig. 7). We previously showed that the initiation of capillary morphogenesis and the maintenance of vessel networks *in vitro* depend on the ECM's resistance to the actin–myosin contractile machinery of ECs,[12] and it is possible that a similar mechanism accounts for our *in vivo* findings. Mammoto *et al.* recently reported that maximal levels of capillary vessel formation were observed *in vivo* in Matrigel substrates with an elastic modulus (E) of 800 Pa (when compared to 700 and 900 Pa substrates).[15] Rheological measurements of our fibrin gels revealed shear elastic moduli (G') of 132 ± 11 Pa for 5 mg/mL gels, 532 ± 37 Pa for 10 mg/mL gels, and 1205 ± 74 Pa for 15 mg/mL gels. However, because fibrin is a complex viscoelastic material that exhibits nonlinear strain-hardening behavior,[16] direct comparisons with Matrigel based on elastic moduli are inappropriate, and the microstructures of these two gels are significantly different. Nevertheless, if we consider these materials as perfectly incompressible, which implies that $3G' << E$, it is noteworthy that optimal neovascularization occurred in fibrin gels whose mechanical properties were of the same order of magnitude as the Matrigel substrates utilized by Mammoto *et al.*

With respect to the second contribution, our data show that codelivery of HUVECs with MSCs was partially capable of overcoming the inhibitory effects of elevated matrix density. This is evident when comparing the results between 10 and 15 mg/mL fibrin, where the differences in functional neovascularization of coculture conditions are minimal despite higher ECM density (Fig. 4C). However, the mere presence of MSCs did not uniformly enhance the quantity of new blood vessels formed across all fibrin concentrations.

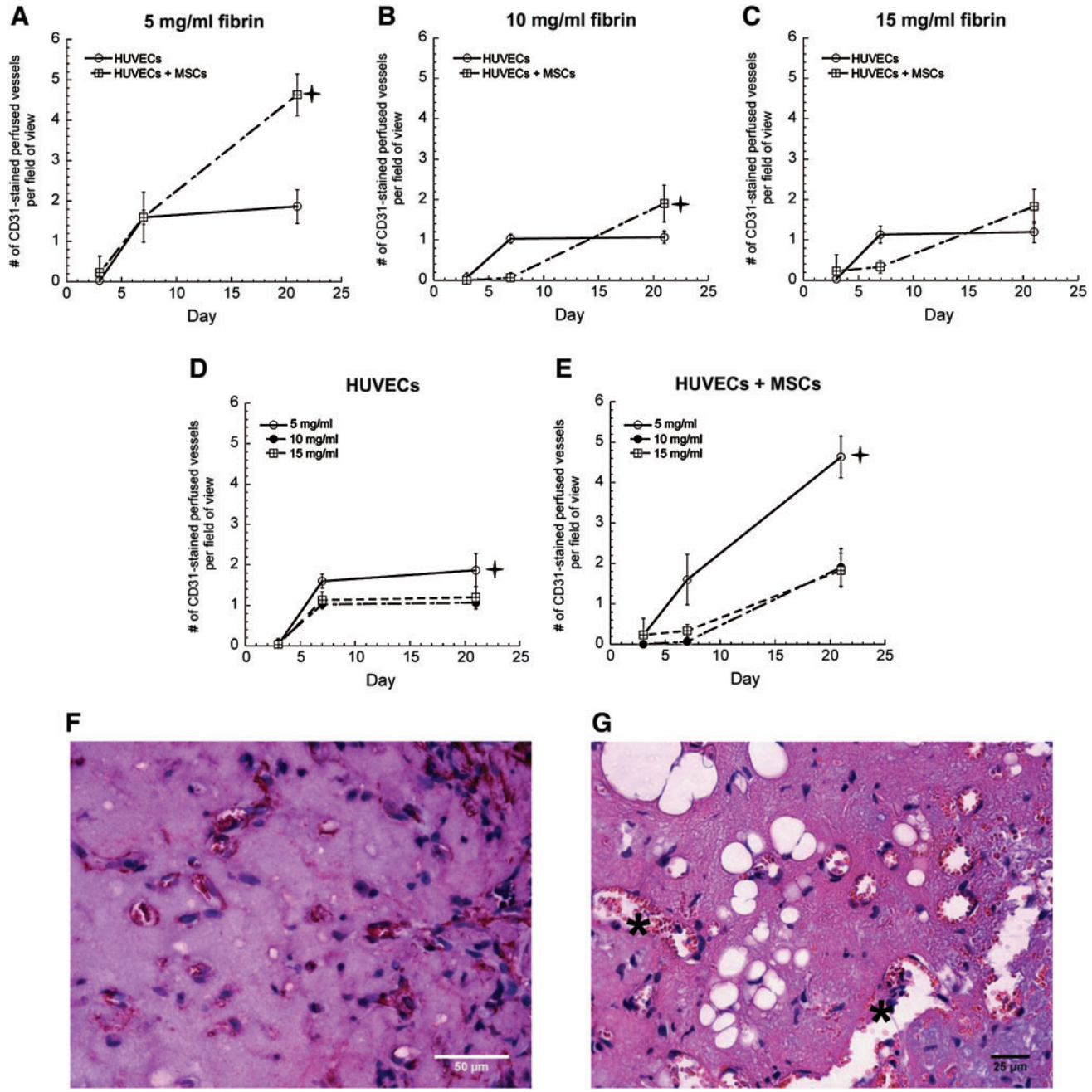

FIG. 4. Quantification of the number of perfused vessels in fibrin-based CD31-stained constructs in **(A)** 5 mg/mL fibrin, **(B)** 10 mg/mL fibrin, **(C)** 15 mg/mL fibrin as a function of the cellular conditions with HUVECs alone (O), and HUVECs+MSCs (□) gels. For panels **(A** and **B)**, ✦ indicates a statistically significant difference ($p < 0.05$) between the HUVECs+MSCs (□) condition and HUVECs alone (O) condition at day 21. The same data are also represented for **(D)** HUVECs alone, and **(E)** HUVECs+MSCs in 5 mg/mL fibrin (O), 10 mg/mL fibrin (●), or 15 mg/mL fibrin (□) at days 3, 7, and 21. For panel **(D)**, ✦ indicates a statistically significant difference ($p < 0.05$) between the 5 mg/mL fibrin (O) condition and 10 mg/mL fibrin (●) condition at day 21. For panel **(E)**, ✦ indicates a statistically significant difference ($p < 0.05$) between the 5 mg/mL fibrin (O) condition relative to the other fibrin conditions at day 21. Representative histology images of perfused constructs at day 21 in **(F)** 5 mg/mL fibrin implants containing HUVECs+MSCs and in **(G)** 5 mg/mL fibrin containing HUVECs alone; asterisks mark extravascular red blood cells. Color images available online at www.liebertonline.com/tea.

While greater numbers of lumen-containing structures were present in HUVEC-MSC coimplant conditions within 5 mg/mL fibrin matrices by day 21 (Fig. 2D), 10 and 15 mg/mL fibrin implants containing HUVECs alone yielded more lumen-containing structures than did HUVEC-MSC coimplants (Fig. 2E, F). A simple explanation for this observation is based on our rationale that it was important to maintain a constant total number of cells (Table 1); therefore, the implants containing both HUVECs and MSC have only half the number of HUVECs present in the HUVEC-only implants (Table 1). However, by looking at the data in Figure 3A–C, we observe that codelivery of HUVECs and MSCs does not

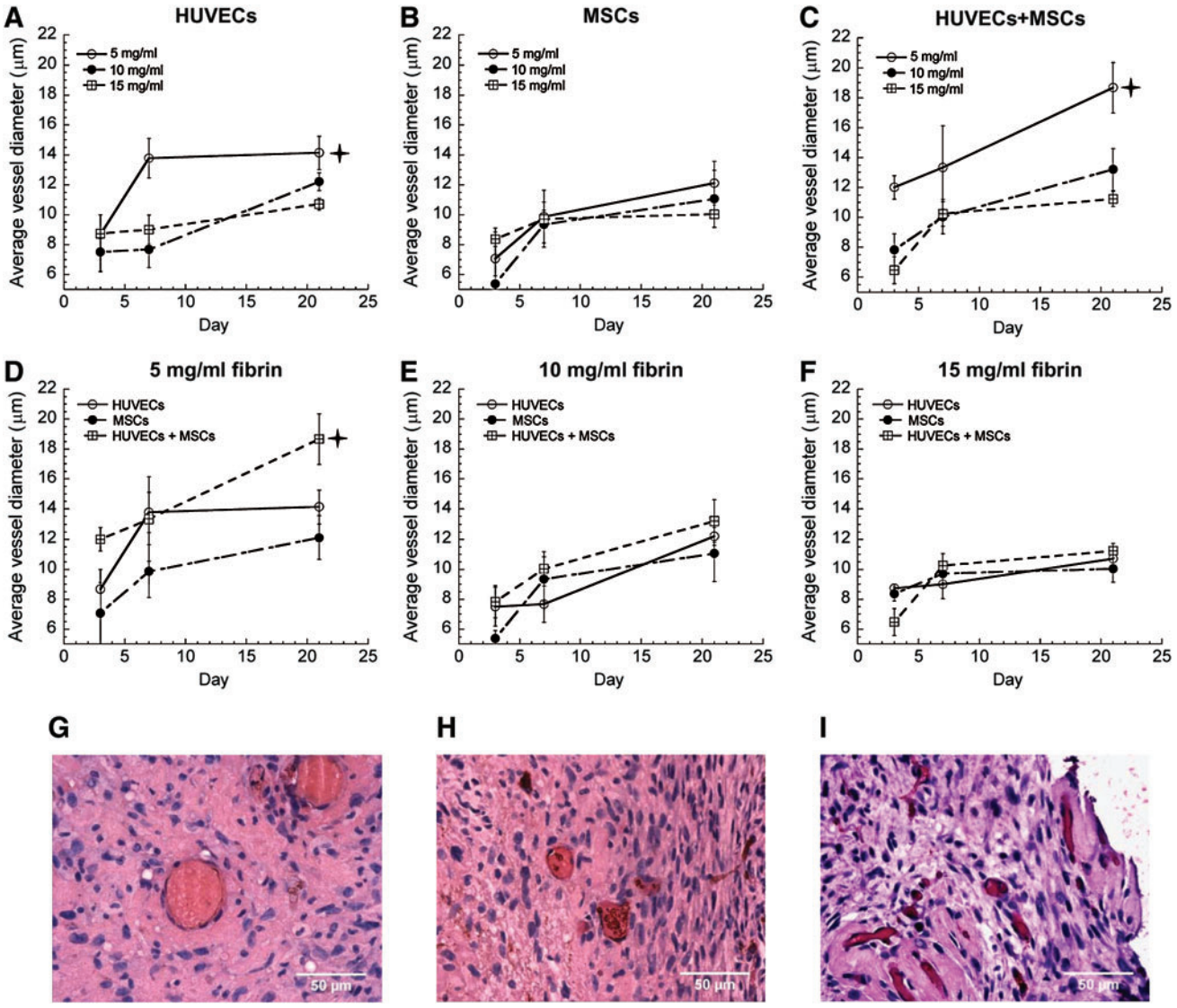

FIG. 5. Vessel diameter quantification in tissue constructs containing **(A)** HUVECs only, **(B)** MSCs only, or **(C)** HUVECs+MSCs in 5 (O), 10 (●), and 15 mg/mL (□) fibrin gels. In panel **(A)**, ✦ indicates a statistically significant difference ($p < 0.05$) between 5 mg/mL fibrin (O) and 15 mg/mL fibrin (□) conditions at day 21; in panel **(C)**, ✦ indicates a statistically significant difference ($p < 0.05$) between the 5 mg/mL condition (O) and the other two concentrations at day 21. The same data are also represented for **(D)** 5 mg/mL fibrin, **(E)** 10 mg/mL fibrin, **(F)** 15 mg/mL fibrin as a function of the cellular conditions, with HUVECs alone (O), MSCs alone (●), or HUVECs+MSCs (□) at days 3, 7, and 21. In panel **(D)**, ✦ indicates a statistically significant difference ($p < 0.05$) between HUVECs+MSCs (□) and the other two conditions at day 21. Representative images on day 21 of capillary vessels formed by codelivery of HUVECs+MSCs in **(G)** 5, **(H)** 10, and **(I)** 15 mg/mL fibrin. Color images available online at www.liebertonline.com/tea.

result in the formation of more human-derived vessels across the range of fibrin concentrations investigated in this study. The metric employed in Figure 3 is more restrictive and specific to vessels derived from the implanted human cells when compared to the metric used in Figure 2 (quantification of total lumen-containing structures). Because the data in Figure 2 may also account for vessels formed by invading mouse cells, it is possible that the higher values in the HUVECs+MSCs condition observed in 5 mg/mL gels (Fig. 2D) may actually reflect increased recruitment of host vessels. It is also possible that cooperation and cross-talk between the two cell types were initially impeded in tissues of higher ECM density. However, and perhaps most importantly, delivery of both cell types always outperformed delivery of a single cell type alone by day 21, regardless of fibrin concentration, in terms of vessel functionality as assessed by quantifying the number of perfused vessels (Fig. 4A–C). Since the data in Figure 4 represent the most restrictive metric (perfused vessels) relative to all those used in the first three figures, we conclude that codelivery of HUVECs with MSCs always led to the generation of the most functional vessels in all three fibrin formulations tested here. The presence of MSCs led to the establishment of more mature vessels as compared to single-cell-type conditions, as demonstrated by the increased size of the perfused vessels (Fig. 5), increased perivascular collagen deposition (Fig. 6), and evidence of MSC differentiation toward stabilizing pericytes expressing smooth muscle markers (Fig. 7).

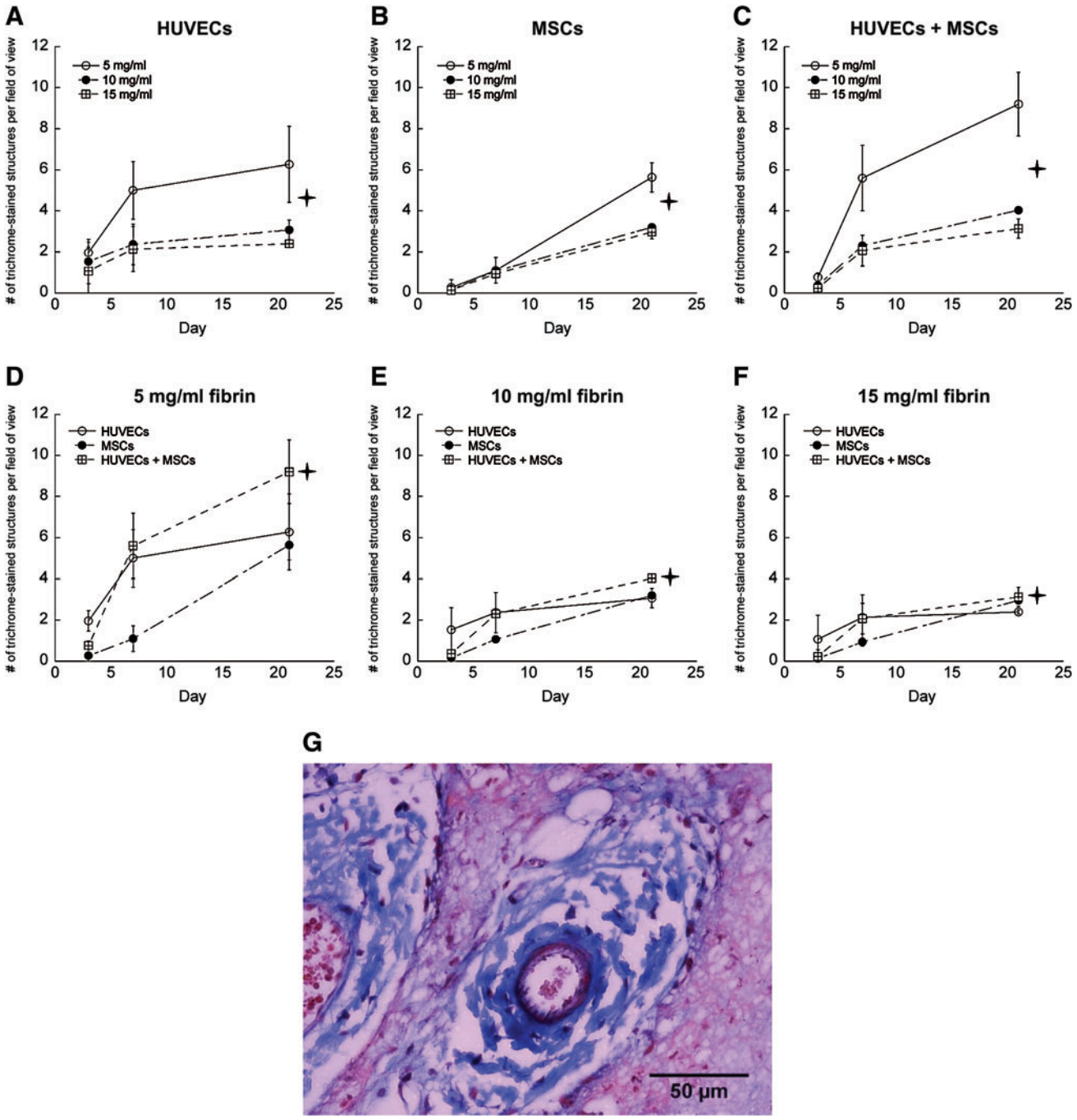

FIG. 6. Perivascular collagen deposition around neovessels formed in tissue implants containing **(A)** HUVECs only, **(B)** MSCs only, or **(C)** HUVECs+MSCs in 5 (O), 10 (●), and 15 mg/mL (□) fibrin gels. In panels **(A** and **B)**, ✦ denotes that the differences between 5 mg/mL fibrin (O) and the other gel concentrations are statistically significant ($p < 0.05$) at day 21, and among all concentrations in **(C)**. The same data are also represented for **(D)** 5 mg/mL fibrin, **(E)** 10 mg/mL fibrin, **(F)** 15 mg/mL fibrin as a function of the cellular conditions, with HUVECs alone (O), MSCs alone (●), or HUVECs+MSCs (□) at days 3, 7, and 21. In panel **(D)**, ✦ indicates a statistically significant difference between the HUVECs+MSCs (□) and MSCs alone (●) conditions. In panel **(E)**, implants containing HUVECs+MSCs (□) exhibit statistically significant differences ($p < 0.05$) in perivascular collagen deposition by day 21, and in **(F)**, between HUVECs+MSCs (□) and HUVECs alone (O), and between HUVECs alone (O) and MSC alone (●). **(G)** A representative day 21 image from a 10 mg/mL fibrin implant containing both cell types. Color images available online at www.liebertonline.com/tea.

Our findings regarding the beneficial effects of MSCs on neovascularization are consistent with many previous reports, and support the hypothesis that the presence of a stromal or mesenchymal cell type capable of differentiating into a pericyte or smooth muscle-like cell stabilizes new vessels. For example, cotransplantation of ECs with 10T1/2 mesenchymal progenitor cells in 3D fibronectin-type I collagen gels yielded stable, long-lasting, and functional blood vessels *in vivo*.[17] Many other studies reinforce the ability of pericytes and other stromal cells to enhance neovascular-

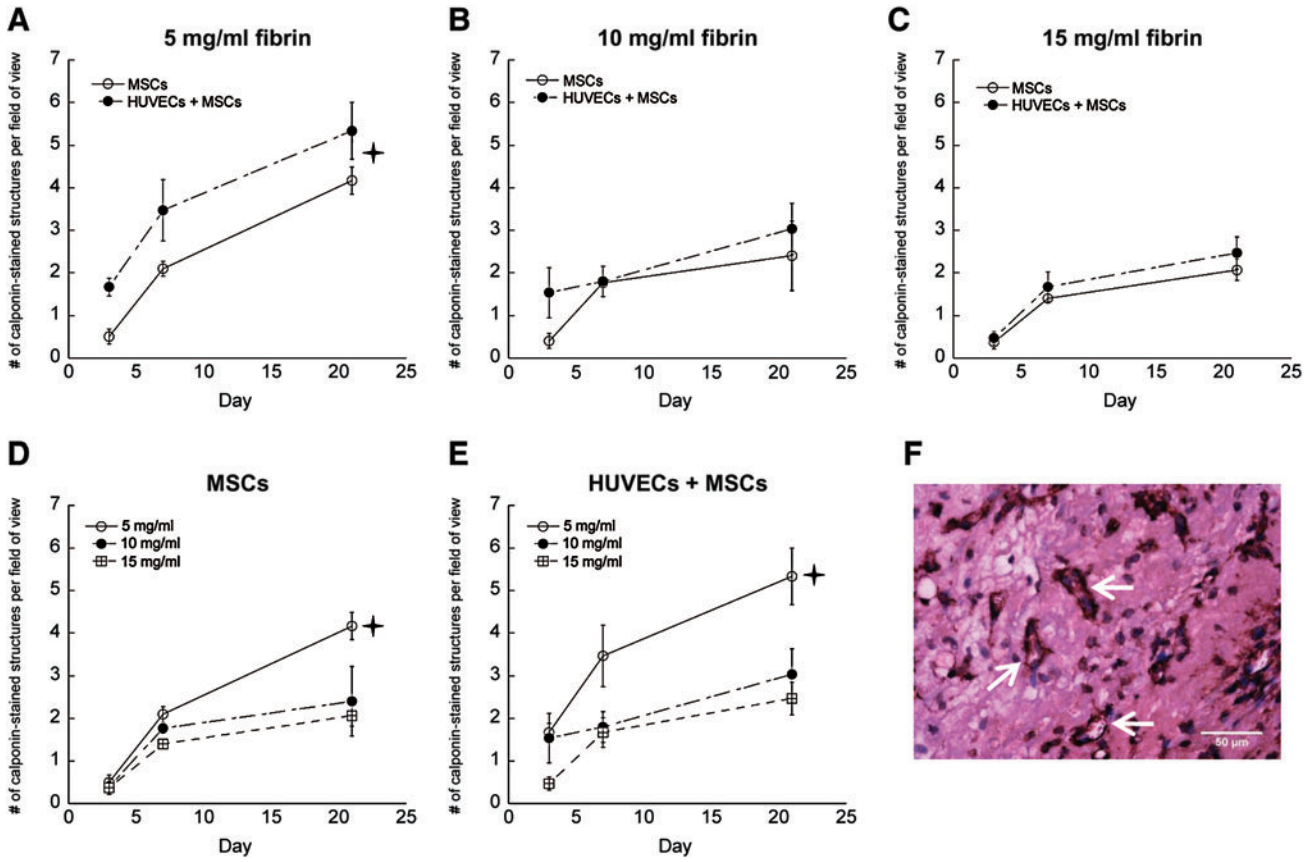

FIG. 7. Vessel structures stained for human calponin in tissue constructs comprised of **(A)** 5 mg/mL fibrin, **(B)** 10 mg/mL fibrin, and **(C)** 15 mg/mL fibrin with either MSCs alone (O) or HUVECs+MSCs (●). The same data are also represented for **(D)** MSCs only and **(E)** HUVECs+MSCs in 5 (O), 10 (●), and 15 mg/mL (□) fibrin gels at days 3, 7, and 21. In panel **(A)**, ✦ indicates a statistically significant ($p < 0.05$) difference between both conditions at day 21. For panels **(D** and **E)**, there is a statistically significant difference ($p < 0.05$) between the 5 mg/mL fibrin-based implants and the other two concentrations at day 21. **(F)** Representative image on day 21 in an implant comprised of 5 mg/mL fibrin and both cell types; arrows identify calponin-stained vessels. Color images available online at www.liebertonline.com/tea.

ization *in vitro* and *in vivo*,[18–24] but the exact mechanisms remain unclear. Inducing 10T1/2 cells to adopt a pericyte phenotype with TGF-β stimulated an angiogenic program of gene expression, with upregulation of several genes implicated in angiogenesis, including VEGF, IL-6, VEGF-C, HB-EGF, CTGF, tenascin C, integrin α5, and Eph receptor A2.[19] MSCs can also secrete an array of proangiogenic factors,[25] and their anatomic location in perivascular niches *in vivo* provides an ideal location for these cells to facilitate tissue repair.[26,27] However, we have also shown that MSCs increase the levels of ECM remodeling enzymes.[11] Their strategic periendothelial locations may facilitate ECM degradation and stabilization of new vessels, without directly increasing vessel quantity, via mechanisms that are distinct from fibroblasts and other cells that can also secrete proangiogenic factors.[13]

Overall, by systematically varying the density of a fibrin-based subcutaneous implant, our study has demonstrated that ECM density regulates neovascularization *in vivo*. Co-delivery of MSCs and ECs *in vivo* led to enhanced vessel functionality and maturation, supporting the idea that delivering both cell types into ischemic tissues may restore tissue perfusion better than delivery of either cell type alone.

Acknowledgments

The authors are grateful to Dr. Christopher Hughes for providing fresh umbilical cords. The authors also thank Dr. Cyrus Ghajar for helping with initial animal experiments as well as insightful discussions. This work was supported by a grant from the NIH (R01 HL085339) and a predoctoral fellowship from the American Heart Association (0815322F to E.K.).

Disclosure Statement

No competing financial interests exist.

References

1. Simons, M., and Ware, J.A. Therapeutic angiogenesis in cardiovascular disease. Nat Rev Drug Discov **2,** 863, 2003.
2. Al Sabti, H. Therapeutic angiogenesis in cardiovascular disease. J Cardiothorac Surg **2,** 49, 2007.
3. Losordo, D.W., and Dimmeler, S. Therapeutic angiogenesis and vasculogenesis for ischemic disease: part II: cell-based therapies. Circulation **109,** 2692, 2004.
4. Harjai, K.J., Chowdhury, P., and Grines, C.L. Therapeutic angiogenesis: a fantastic new adventure. J Interv Cardiol **15,** 223, 2002.

5. Ingber, D.E., and Folkman, J. How does extracellular matrix control capillary morphogenesis? Cell **58,** 803, 1989.
6. Sieminski, A.L., Hebbel, R.P., and Gooch, K.J. The relative magnitudes of endothelial force generation and matrix stiffness modulate capillary morphogenesis *in vitro*. Exp Cell Res **297,** 574, 2004.
7. Deroanne, C.F., Lapiere, C.M., and Nusgens, B.V. *In vitro* tubulogenesis of endothelial cells by relaxation of the coupling extracellular matrix-cytoskeleton. Cardiovasc Res **49,** 647, 2001.
8. Vailhe, B., Lecomte, M., Wiernsperger, N., and Tranqui, L. The formation of tubular structures by endothelial cells is under the control of fibrinolysis and mechanical factors. Angiogenesis **2,** 331, 1998.
9. Nehls, V., and Drenckhahn, D. A novel, microcarrier-based *in vitro* assay for rapid and reliable quantification of three-dimensional cell migration and angiogenesis. Microvasc Res **50,** 311, 1995.
10. Ghajar, C.M., Chen, X., Harris, J.W., Suresh, V., Hughes, C.C., Jeon, N.L., Putnam, A.J., and George, S.C. The effect of matrix density on the regulation of 3D capillary morphogenesis. Biophys J **94,** 1930, 2008.
11. Ghajar, C.M., Blevins, K.S., Hughes, C.C., George, S.C., and Putnam, A.J. Mesenchymal stem cells enhance angiogenesis in mechanically viable prevascularized tissues via early matrix metalloproteinase upregulation. Tissue Eng **12,** 2875, 2006.
12. Kniazeva, E., and Putnam, A.J. Endothelial cell traction and ECM density influence both capillary morphogenesis and maintenance in 3-D. Am J Physiol Cell Physiol **297,** C179, 2009.
13. Ghajar, C.M., Kachgal, S., Kniazeva, E., Mori, H., Costes, S.V., George, S.C., and Putnam, A.J. Mesenchymal cells stimulate capillary morphogenesis via distinct proteolytic mechanisms. Exp Cell Res **316,** 813, 2010.
14. Griffith, C.K., Miller, C., Sainson, R.C., Calvert, J.W., Jeon, N.L., Hughes, C.C., and George, S.C. Diffusion limits of an *in vitro* thick prevascularized tissue. Tissue Eng **11,** 257, 2005.
15. Mammoto, A., Connor, K.M., Mammoto, T., Yung, C.W., Huh, D., Aderman, C.M., Mostoslavsky, G., Smith, L.E.H., and Ingber, D.E. A mechanosensitive transcriptional mechanism that controls angiogenesis. Nature **457,** 1103, 2009.
16. Janmey, P.A., Winer, J.P., and Weisel, J.W. Fibrin gels and their clinical and bioengineering applications. J R Soc Interface **6,** 1, 2009.
17. Koike, N., Fukumura, D., Gralla, O., Au, P., Schechner, J.S., and Jain, R.K. Tissue engineering: creation of long-lasting blood vessels. Nature **428,** 138, 2004.
18. Hirschi, K.K., Rohovsky, S.A., and D'Amore, P.A. PDGF, TGF-beta, and heterotypic cell-cell interactions mediate endothelial cell-induced recruitment of 10T1/2 cells and their differentiation to a smooth muscle fate. J Cell Biol **141,** 805, 1998.
19. Kale, S., Hanai, J., Chan, B., Karihaloo, A., Grotendorst, G., Cantley, L., and Sukhatme, V.P. Microarray analysis of *in vitro* pericyte differentiation reveals an angiogenic program of gene expression. FASEB J **19,** 270, 2005.
20. Ding, R., Darland, D.C., Parmacek, M.S., and D'Amore, P.A. Endothelial-mesenchymal interactions *in vitro* reveal molecular mechanisms of smooth muscle/pericyte differentiation. Stem Cells Dev **13,** 509, 2004.
21. Darland, D.C., and D'Amore, P.A. TGF beta is required for the formation of capillary-like structures in three-dimensional cocultures of 10T1/2 and endothelial cells. Angiogenesis **4,** 11, 2001.
22. Kaigler, D., Krebsbach, P.H., Polverini, P.J., and Mooney, D.J. Role of vascular endothelial growth factor in bone marrow stromal cell modulation of endothelial cells. Tissue Eng **9,** 95, 2003.
23. Shepherd, B.R., Jay, S.M., Saltzman, W.M., Tellides, G., and Pober, J.S. Human aortic smooth muscle cells promote arteriole formation by coengrafted endothelial cells. Tissue Eng A **15,** 165, 2009.
24. Melero-Martin, J.M., De Obaldia, M.E., Kang, S.Y., Khan, Z.A., Yuan, L., Oettgen, P., and Bischoff, J. Engineering robust and functional vascular networks in vivo with human adult and cord blood-derived progenitor cells. Circ Res **103,** 128, 2008.
25. Wagner, J., Kean, T., Young, R., Dennis, J.E., and Caplan, A.I. Optimizing mesenchymal stem cell-based therapeutics. Curr Opin Biotechnol **20,** 531, 2009.
26. Caplan, A.I. All MSCs are pericytes? Cell Stem Cell **3,** 229, 2008.
27. Crisan, M., Yap, S., Casteilla, L., Chen, C.W., Corselli, M., Park, T.S., Andriolo, G., Sun, B., Zheng, B., Zhang, L., Norotte, C., Teng, P.N., Traas, J., Schugar, R., Deasy, B.M., Badylak, S., Buhring, H.J., Giacobino, J.P., Lazzari, L., Huard, J., and Peault, B. A perivascular origin for mesenchymal stem cells in multiple human organs. Cell Stem Cell **3,** 301, 2008.

Address correspondence to:
Andrew J. Putnam, Ph.D.
Department of Biomedical Engineering
University of Michigan
2154 Lurie Biomedical Engineering
1101 Beal Ave.
Ann Arbor, MI 48109-2110

E-mail: putnam@umich.edu

Received: May 5, 2010
Accepted: October 27, 2010
Online Publication Date: December 1, 2010